INT. J. NUM. METH. HEAT FLUID FLOW, VOL. 5, 63–74 (1994)

ACCURATE ANIMATION OF THE THERMO-FLUIDIC PERFORMACE OF THE PRESSURE-WAVE MACHINE AND ITS BALANCED MATERIAL OPERATION

H. OBERHEM** AND H. A. NOUR ELDIN*

*Group of Automatic Control and Technical Cybernetics, University of Wuppertal D-42097 Wuppertal 1, Germany and
**Department of Production Control, Bayer AG, Dormagen, Germany

ABSTRACT

Modelling, computation and performance animation of turbomachinery systems has recently enjoyed remarkable attention in *CAD* research. This is also reflected its application to exhaust machine components such as turbo loaders and the exceptionally novel pressure wave machine (Comprex) in the automobile industry and gas turbines. The necessity for the thermo-fluidic performance animation of such pressure wave machines results from the fact that the machine geometry must be adapted to the technical and thermo-fluidic properties of the exhaust flow of the gas turbine or automobile engine. Experimental adaptation or adjustment is costly and should be validated for every application case. Thus the potential to apply accurate animation for such shock-tube like behaviour of compressible flow is now economically promising with a view to optimizing the design of the pressure wave machine. This paper presents briefly the problem oriented algorithms used and illustrates the performance animation of the pressure wave machine operating under constant speed drive. After introducing the pressure wave machine operation, the principles and summary of the algorithms used to compute the thermodynamic behaviour within the cell, the boundary models and the accuracy of computation. A Comprex cycle operating on an engine exhaust gas with $T = 920°K$, $p = 2bar$ is illustrated through 3-dimensional representations for pressure, speed of flow and temperature. The particle path (gas and air) together with time representation of the state variables at different points of the Compex will be shown. The mass balance problem is discussed and the conditions for mass balanced flow for the gas as well as for the air side are given. The results achieved for such materially balanced pressure wave machines indicate a reduction in the costs for subsequent experimental validation and to deliver the sound base for further development towards considering the pre-balanced transient operation cases as well.

KEY WORDS Modelling Turbomachines *CAD* Pressure waves machines

INTRODUCTION

Exhaust machine components and systems have been used as gas (air) loaders for a long time, especially for Diesel engines[1]. The most popular type of such exhaust machines in the turboloader, by which higher total motor power is achievable[2]. Its resulting loading pressure is almost proportional to the rotor speed, and thus to the motor speed. As a result, enhancing the total motor power at low motor speeds is scarcely achievable. Besides, the acceleration time response of the turbo-loaded motor is slow as a good part of the exhaust gas energy is required to accelerate the rotor. It is thus not surprising, that most of the technological improvements concerning turbo-loaders are related to these two performance points.

0961–5539/95/010063–12$2.00

Received October 1993
Revised April 1994

The novel alternative for turbo loaders is the pressure wave machine 'Comprex'[3,4,5,6,7,8,9,10,11,12] Originally, it was conceived as an upper stage for gas turbines[7]. In contrast to the mechanical turbo loaders, the energy exchange in the 'Comprex' is exploited directly through unstationary (compression; expansion) pressure waves[8,13,14,15] propagating with the speed of sound. The above mentioned performance drawbacks of mechanical loaders are thus avoided.

In his patent[4], Seippel demonstrated how an extraordinary intuitive understanding of compressible flow can lead to the construction of a functioning pressure wave machine, named 'Comprex'. It was firstly used as an upper stage in a gas turbine plant[8]. De Haller[16] and Jenny[17] analysed and calculated the thermofluidic phenomena in the Comprex. Beginning in 1956, BBC (now ABB) adapted the pressure wave machine to the automative drives, where it had been successful for Diesel trucks. By 1969, Comprex prototypes for car drives were set in for durability experiments.

PRINCIPLES OF COMPREX OPERATION CONDITIONS

Figure 1 shows the principle components of the Comprex in connection to the motor-drive[18]. For a given motor speed, it is convenient to represent the cell drum as expanded over one cycle of rotation (*Figure 2*). Compression waves are represented by the bold lines, while expansion waves are indicated by dashed lines. For the so called 'complete trimmed process'[11], whose thermodynamic state diagram is shown in *Figure 3*, the main aspects of the Comprex operation will be briefly addressed here.

a) *High pressure phase*

a.1: *Opening of the high pressure gas channel*
A pressure wave (I_L) results. Air will be compressed and hot gas particles enter the cell.

a.2: *Opening of the high pressure air channel*
Ideal opening time should coincide with the arrival of the high pressure wave[11]. This timing is important for the efficiency of the Comprex.

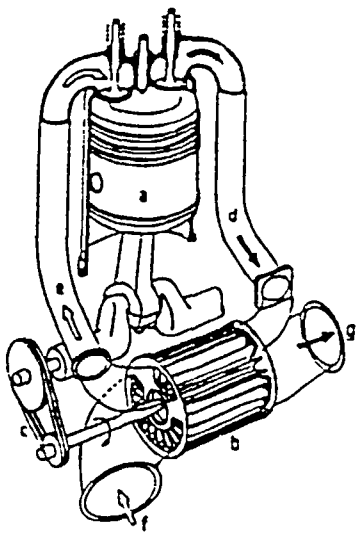

Figure 1 Schematic illustration: pressure wave machine-motor[3]. a – motor, b – cell drum exhaust, c – belt drive, d – high pressure exhaust, e – high pressure-air, f – high pressure-air, g – low pressure-air

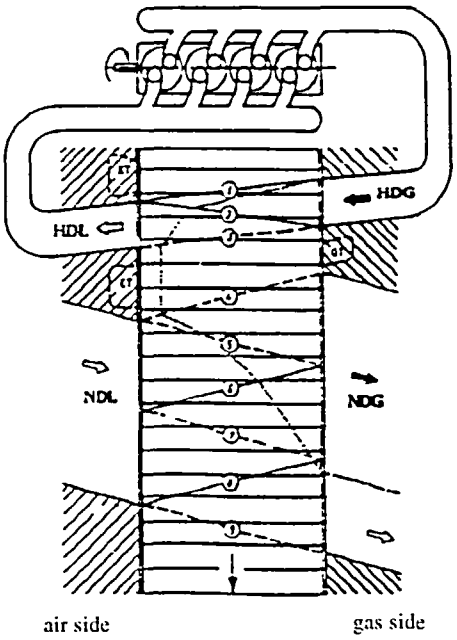

Figure 2 Schematic illustration: cell drum expanded over one cycle of rotation[3]

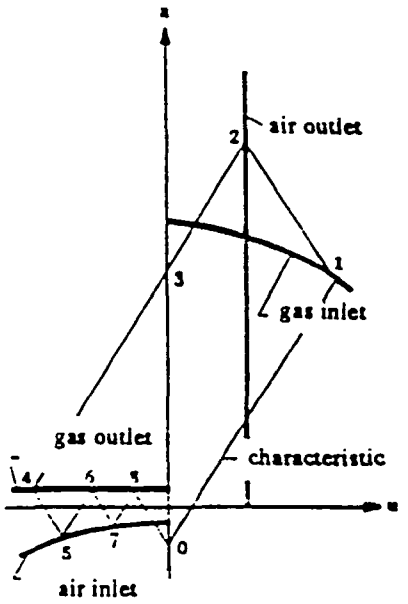

Figure 3 State diagram[19] for graphical determination of state variables in the (*a*-*u*)-diagram

a.3: *Closure of high pressure gas channel*
This should be timed with the arrival of the reflected pressure wave. No gas particle back streaming is thus achievable. This condition is important for efficient trimmed process[11].

a.4: *Closure of high pressure air channel*
Ideal closure should coincide with the arrival of the expansion wave. This is the third condition for a completely trimmed process[11].

b) *Low pressure phase*

For opening and closing the low pressure gas or air-channels, another set of trimming rules is necessary in order to initiate a strong gas expansion wave that expells gas particles to the low pressure gas channel. When the gas expansion reaches the air side, the resulting air stream is strong enough to let the cell gas stream out and fresh air stream into the cell. Reference 11, 18 and 19 can be further consulted for trimming details of this low pressure process. Also boundary improvements in form of expansion cavity, compression cavity and gas cavity are necessary for Comprex application in automotive drives[11,18,19]. However, these aspects will not be presented in this paper.

THE NONSTATIONARY COMPRESSIBLE FLOW IN THE PRESSURE WAVE MACHINE (COMPREX)

The one dimensional unsteady gas flow with friction, heat transfer, variable entropy and gradual area changes can be described by the continuity, momentum and energy equations[1,2,3,17,18] in

differential form:

continuity equation:

$$\rho_t + u\rho_x + \rho u \frac{1}{F}\frac{\mathrm{d}F}{\mathrm{d}x} = 0 \tag{1}$$

F: tube area
x: space variable
t: time variable

momentum equation:

$$u_t + uu_x + \frac{1}{\rho}p_x + w = 0 \tag{2}$$

$$w = \frac{\lambda}{2D}\frac{u}{|u|}u^2 \tag{2a}$$

λ: friction factor
D: tube diameter

energy equation:

$$p_t - \frac{\kappa p}{\rho}\rho_t + up_x - \frac{\kappa p u}{\rho}\rho_x - (\kappa - 1)(q + \rho u w) = 0 \tag{3}$$

κ: isentropic coefficient
q: heat transfer

The analytic solution for the material speed $u(x, t)$, pressure $p(x, t)$ and density $\rho[x, t]$ can be deduced following the argumentation in[17,21] through the equation:

$$\begin{bmatrix} u\,\mathrm{d}t - \mathrm{d}x & \frac{1}{\rho}\mathrm{d}t & 0 \\ \rho\,\mathrm{d}t & 0 & u\,\mathrm{d}t - \mathrm{d}x \\ 0 & u\,\mathrm{d}t - \mathrm{d}x & -\kappa\frac{p}{\rho}(u\,\mathrm{d}t - u\,\mathrm{d}x) \end{bmatrix} \begin{bmatrix} u \\ p \\ \rho \end{bmatrix} = \begin{bmatrix} -w\,\mathrm{d}t - \mathrm{d}u \\ -\rho u \frac{1}{F}\frac{\mathrm{d}F}{\mathrm{d}x}\mathrm{d}t - \mathrm{d}\rho \\ (\kappa - 1)(\rho u w + q)\,\mathrm{d}t - \mathrm{d}p\frac{\kappa p}{\rho}\mathrm{d}\rho \end{bmatrix} \tag{4}$$

as quotients of determinants[17,18]. The general direction condition is obtained when the determinant of (4) vanishes, thus:

$$[u\,\mathrm{d}t - \mathrm{d}x]^2 = \frac{\kappa p}{\rho}\mathrm{d}t^2 = a^2\mathrm{d}t^2 \tag{5}$$

The three directions of characteristic at point p are:

$$\left(\frac{\mathrm{d}x}{\mathrm{d}t}\right)_2 = u, \qquad \left(\frac{\mathrm{d}x}{\mathrm{d}t}\right)_{1,3} = u + a \tag{6}$$

The above directions are usually called 'disturbances lines' or 'mach-lines'. Jenny[17] derived the differential form of the solutions of equation[4] and has shown that the resulting conditions of two determinants are identical. His graphical method for the design and analysis of machines with one dimensional unsteady gas flow used these two equations. In his dissertation Oberham[18], succeeded to render the general compatibility condition using the third determinant. In its

differential form, the generalized compatibility condition[18] is:

$$\det\begin{pmatrix} u\,dt - dx & \frac{1}{\rho}dt & -w\,dt - du \\ \rho\,dt & 0 & -\rho u\frac{1}{F}\frac{dF}{dx}dt - d\rho \\ 0 & u\,dt - dx & (\kappa-1)(\rho u w + q)\,dt - dp + \frac{\kappa p}{\rho}d\rho \end{pmatrix} = 0 \tag{7}$$

Expanding this determinant and ordering of terms lead to the *general compatibility condition*[18]:

$$dp - \left(\rho u - \rho\frac{dx}{dt}\right)du + \left[\left(u - \frac{dx}{dt}\right)^2\frac{\kappa p}{\rho}\right]\cdot$$
$$d\rho - (\kappa-1)\,dtq\left[\left(u - \frac{dx}{dt}\right)\rho\,dt + (\kappa-1)\rho u\,dt\right]\cdot$$
$$w + \left(u - \frac{dx}{dt}\right)^2\rho u\,dt\frac{1}{F}\frac{dF}{dx} = 0 \tag{8}$$

With the compatibility condition (8) along the corresponding characteristic directions (6), the main equations for the numerical computation of the one dimensional compressible gas flow have been given in differential form[18,20].

Wave propagation and state variable relations at pressure wave discontinuities

The basic equations for directions and compatibility conditions are valid almost to the continuity limit that can occur during the shock waves. For the compressible flow near pressure wave discontinuity however, the characteristics contact each other (shock wave case). The discontinuity of the states lead to ambiguous results. Sauer[21] proposed the additional considerations to determine the speed of propagation and the state variable relations across the shock front. Based on his treatment, and using the Rankine–Hugoniot equations, the state conditions across a shock wave were derived:

a) *shock wave speed*:

$$c_{1,2} = -e/2 \pm \sqrt{\frac{e^2}{4} + f} \tag{9}$$

with

$$e = \tfrac{1}{2}[(\kappa-3)u_b - (\kappa+1)u_a] \tag{10}$$
$$f = \tfrac{1}{2}[(\kappa-1)u_b - (\kappa+1)u_a] + a_b^2 \tag{11}$$

The positive sign in (9) is for the *right* travelling shock wave with the speed c_1 while the negative sign is for the left travelling shock wave with speed c_2.

b) *pressure ratio*:

$$\frac{p_b}{p_a} = 1 + 2\frac{\kappa}{\kappa+1}\left[\left(\frac{c}{a_b}\right)^2 - 1\right] \tag{12}$$

$$\frac{p_v}{p_b} = 1 - 2\frac{\kappa}{\kappa+1}\left[1 - \left(\frac{a_b}{c}\right)^2\right] \tag{13}$$

The set of equations (9–13) complement the dynamics of incompressible flow within the pressure wave machine (complex) completely. What is now required, before the numerical solution, is the information about the types of waves accruing within the cell. For this purpose, the following decision rules are cast in a disturbance index[18,20,22] to identify the type and direction of propagated waves within the pressure wave machine:

$$u_0 = \frac{p_1 - p_3 + a_1\rho_1 u_1 + a_3\rho_3 u_3}{a_1\rho_1 + a_3\rho_3} \tag{14}$$

$$\Delta u = |u_0 - u_3| - |u_0 - u_1| \tag{15}$$

$$\Delta p = p_1 - p_3 \tag{16}$$

$$\text{sign}(\Delta u) = \text{sign}(\Delta p) \quad \text{compression wave} \tag{17}$$

$$\text{sign}(\Delta u) \neq \text{sign}(\Delta p) \quad \text{expansion wave} \tag{18}$$

$$\text{sign}(\Delta u) > 0 \quad \text{right travelling wave} \tag{19}$$

$$\text{sign}(\Delta u) < 0 \quad \text{left travelling wave} \tag{20}$$

With the sign test, it is possible to determine the type of the wave acting on (t_0, x_0).

The discretization for direction and compatibility conditions

The basic analytic equation (6) for the characteristics through an arbitrary point as well as the corresponding compatibility conditions along these characteristics[18,20,22] offer both locality and physical interpretation of the dynamic equations. By discretizing these system of equations for every three points, a nonlinear equation in five unknown variables: position x_k, t_k, and states u_k, p_k, ρ_k is obtained. Applying a finite different approximation to the compatibility conditions in its integral form[18,20,22] and using a second oder approximation for the integrals leads to the following nonlinear equations[18,22]

$$(p_0 - p_1) + \tfrac{1}{2}(a_1\rho_1 + a_0\rho_0)(u_0 - u_1) - \tfrac{1}{2}(E_1^* + E_{0I}^*)(t_0 - t_2) = 0 \tag{22}$$

$$(p_0 - p_2) + \tfrac{1}{2}(a_2^2 + a_0^2)(\rho_0 - \rho_2) - \tfrac{1}{2}(E_2^* + E_{0II}^*)(t_0 - t_2) = 0 \tag{23}$$

$$(p_0 - p_3) + \tfrac{1}{2}(a_3\rho_3 + a_0\rho_0)(u_0 - u_3) - \tfrac{1}{2}(E_3^* + E_{0III}^*)(t_0 - t_3) = 0 \tag{24}$$

where E_1^*, E_2^*, E_3^* are nonlinear disturbance terms at the points 1, 2, 3 respectively while E_{0I}^*, E_{0II}^*, E_{0III}^* disturbance terms at point P_0 for corresponding lines,[18,22]. Equations (22–24) are the basic nonlinear equations for the variable grid method. In order to achieve robustness in the convergence when a Newton–Raphson Algorithm is used, a first order approximation was derived to obtain the starting values of the states[18,22]. Also, it is necessary to reorganize the grid after a certain limit of computation steps. A grid reorganization step is introduced to the pure variable grid method in order to attain a homogeneous grid. For the pressure wave machines, the number of grid organizations did not get higher than four grid organization steps.

Test for the accuracy of numerical computations within the pressure wave cell

The accuracy of the variable grid method has been checked for the case of a shock tube, as the numerical solution can be compared with semi-analytical methods. For an infinite value problem, a shock tube of infinite length was considered, so that reflections are excluded. The test results for the open sided shock tube case are documented in reference 18 and shown in reference 22.

The main aspects are mentioned here briefly: After 13 ms, the difference at the temperature is less than 0.5 degrees and the difference in the pressure is 10 mbar. Also the material speed

accuracy is within 1 m/s. The shock wave side of solution was shown at 1.5 m. The sharpness of the pressure, material and temperature discontinuities is sustained. This is in contrast to the known results out of the fixed grid difference methods where damped oscillations appear at the discontinuity sides. One can summarize the solution accuracy at $x = 1{,}5$ m of the expansion side as well as the compression side by noting the maximal error[18,22]:

Compression side	Numerical	Analytical	Error
shock wave speed	456.62 (m/s)	459.98 (m/s)	0.73%
pressure p	1.946 (bar)	1.929 (bar)	0.88%
temperature T	353.7 K	356.4 K	0.76%
material speed	168.6 m/s	169.85 m/s	0.73%

Expansion side: Pressure $p = 0.98\%$, Temperature $T = 0.29\%$, Material speed $u = 1.33\%$

The boundary models for inflow and outflow

The closed boundary phase was animated by generating a new grid point at the boundary. The time of generation of this boundary point as well as the computation of its gas states are computed by two compatibility conditions only as the state speed u at the boundary is identically zero. An auxiliary supporting grid point – outside the cell – is introduced having the same state variable values as the nearest grid point used for computation, but with opposite wave propagation direction. The nonlinear equations for closed boundary are thus[18]:

$$(p_0 - p_1) - \tfrac{1}{2}(a_1\rho_1 + a_0\rho_0)u_1 - \tfrac{1}{2}(E_1^* + E_0^*)(t_0 - t_1) = 0 \tag{25}$$

$$(p_0 - p_2) - \tfrac{1}{2}(a_2^2 + a_0^2)(\rho_0 - \rho_2) - \tfrac{1}{2}(E_2^* + E_0^*)(t_0 - t_2) = 0 \tag{26}$$

$$(p_0 - p_3) - \tfrac{1}{2}(a_3\rho_3 + a_0\rho_0)u_3 - \tfrac{1}{2}(E_3^* + E_0^*)(t_0 - t_3) = 0 \tag{27}$$

For a left boundary, equations (26) and (27) are used while equations (25) and (26) are used for the right side boundary.

For outflow or inflow cases, corresponding models were implemented and incorporated in a manner that animates the particle flow by expelling grid points at outflow and inserting new grid points at inflow case[18,20].

SIMULATION AND ANIMATION FOR THE PRESSURE WAVE MACHINE PERFORMANCE UNDER GIVEN BOUNDARY CONDITION

As the boundary geometry is the main adjustment and design parameter for adapting the pressure wave machine to a new application, it is not only necessary to compute the physical variables in the Comprex, but also let them be animated in a manner suitable for a designer using a *CAD*-animated pressure wave machine. This software package has been implemented on a *CYBER* 170 using 41 grid original points. With five grid reorganization steps, a Comprex cycle was animated within 9.6 seconds[18]. Besides curve or function illustrations, a video film can be produced to illustrate the dynamic performance of the Comprex, that indicates to the design engineer the dynamic effects occurring in the Comprex due to variation of the Comprex design parameters[18].

Figure 4 shows the boundary geometry (opening and closing angles) together with the boundary conditions for one complete Comprex cycle. *Figures 5, 6* and *7* show the three-dimensional illustration of the dynamic performance of the pressure p, particle speed u and temperature T for a complete Comprex cycle. The analysis of such dynamic performance is given briefly here:

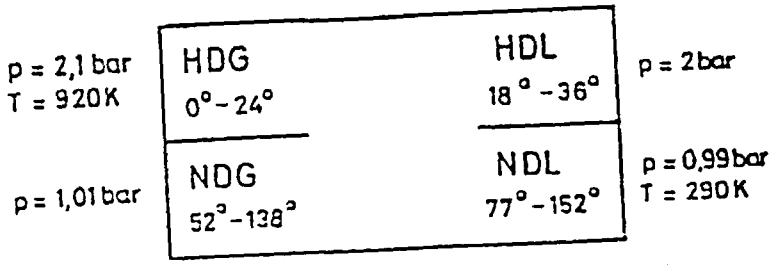

Figure 4 The boundary geometry with the boundary conditions

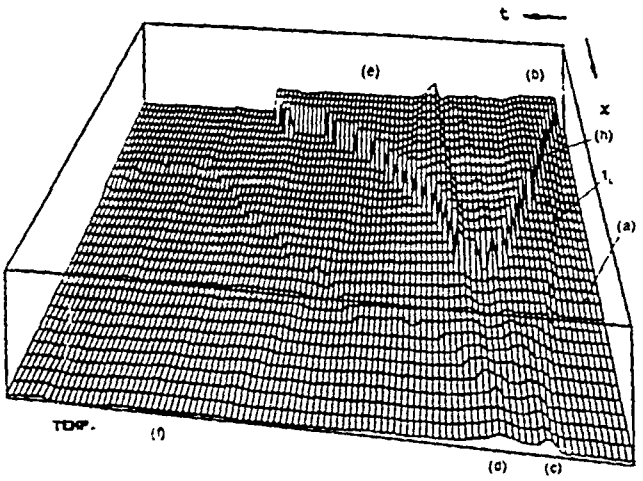

Figure 5

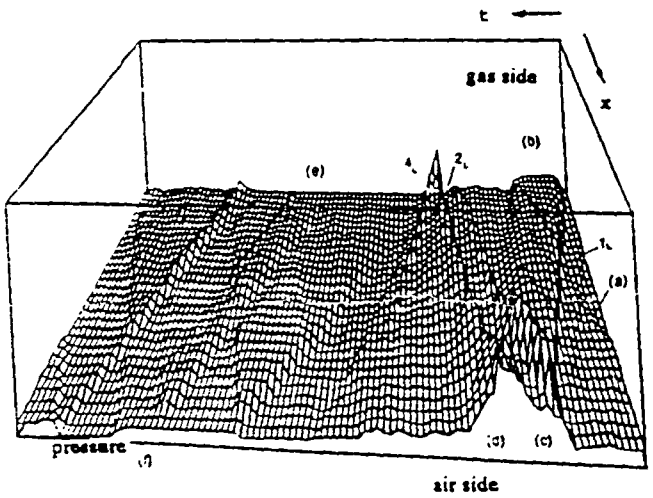

Figure 6

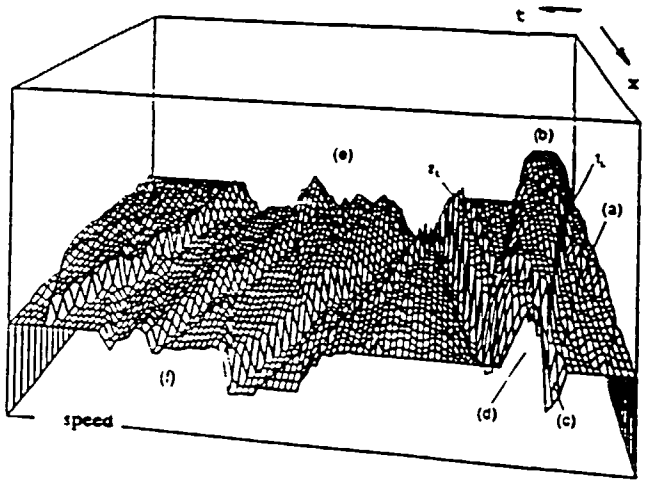

Figure 7

a) *High pressure phase*

A gas pressure wave (I_L) propagates towards the air side. Just before its arrival, the air high pressure channel is opened. Due to such inadequate timing, air enters the cell but will be compressed thereafter (*Figure 6*). The corresponding temperature rise (*Figure 7*) is moderate in comparison to gas to fresh air wave front temperature. With closure of both high pressure channels, an undesired strong pressure wave (2_L) is induced.

b) *Low pressure phase*

With opening of the gas low pressure channel (*Figure 6*), a strong expansion wave (4_L) builds up and propagates to the air side. The material front (gas-air) propagates in the opposite direction. Opening of the low air pressure channel causes some auxiliary waves. The Comprex cell is relieved from the rest of the gas (in ideal case) and is being filled with fresh air. With the closure of both channels, some new waves arise, before the cell returns to its original state at the beginning of the cycle.

From the brief analysis above, one notices that besides the 'main waves', a remarkable number of auxiliary waves that propagate, reflect and cross over each other. The accurate computation of the unstationary compressible flow by the variable grid method is capable of dealing with such complex wave processes. Its adaptability to those waves occurring is demonstrated by the supporting grid (*Figure 8*). The supporting grid points in *Figure 8* show the variation of grid points location in dependence on the dynamics and the waves in the cell. They may be also interpreted as a 'particle path'. One also observed the necessary grid reorganization. The insertion of new grid supporting points whenever particles are coming into the cell as well as the excretion of the grid points whenever the particles are expelled out of the Comprex is illustrated clearly in *Figure 9*. In *Figure 9* the particle path is computed showing gas or air particles streaming inside and outside the Comprex. The flow states at $x = 0$ and $x = 1$ are shown as a function of time in *Figures 10* and *11*. The consequences of pre-timed opening (at 0.19 ms) can be studied exactly. Material discontinuities, pressure discontinuities (*Figure 10*) as well as discontinuous material speed reversal (*Figure 11*) are accurately computed without any unphysical oscillations. This fact is clearly illustrated through the time flash of the distribution of the pressure, temperature and particle speed over the cell (*Figure 12*). Such accuracy of Comprex animation is desired in order to achieve the optimum design of the Comprex cell geometric boundary and opening angles.

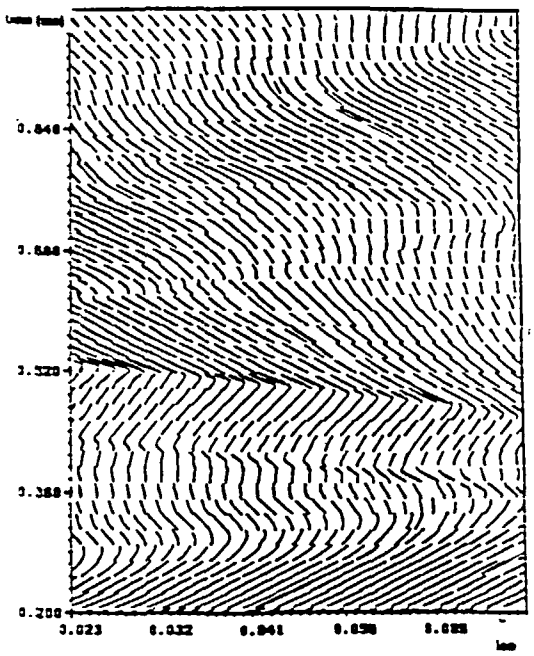

Figure 8

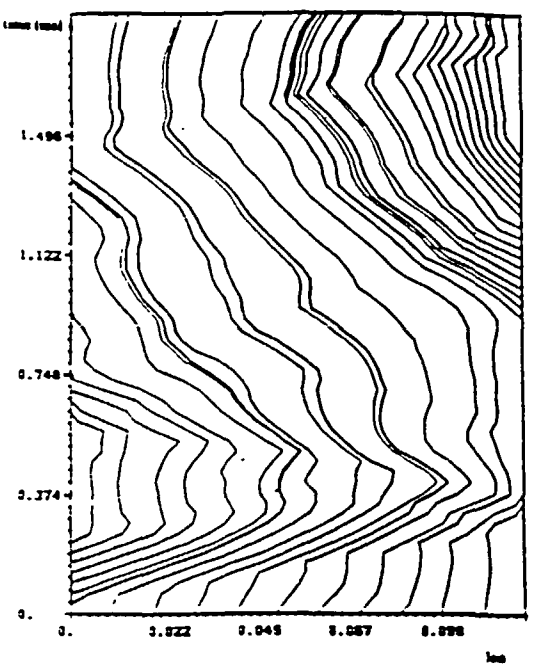

Figure 9

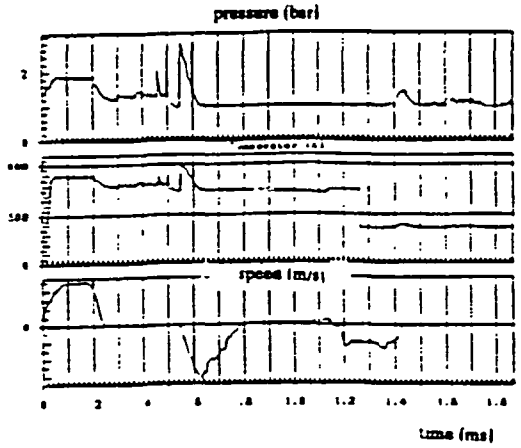

Figure 10

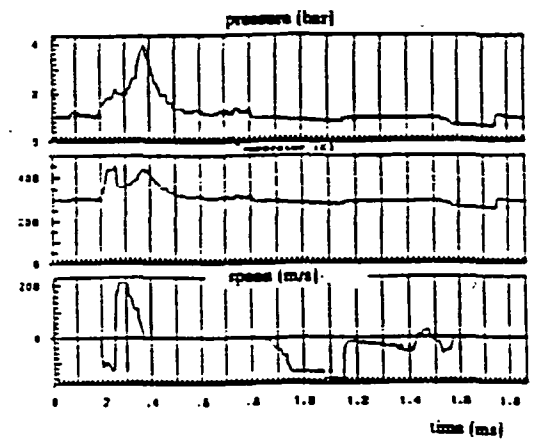

Figure 11

THE BALANCE OF MATERIAL OPERATION CONDITIONS

For a proper Comprex motor operation, it is necessary that the gas and air materials are balanced. Otherwise, the motor cannot be loaded properly. Computing a materially balanced Comprex has been very tedious and inaccurate. Besides, they could not be arranged to be automated. Through the variable grid method[18], however, such balancing is adequately automated. The material and energy balance is parametrized through the physical variables at

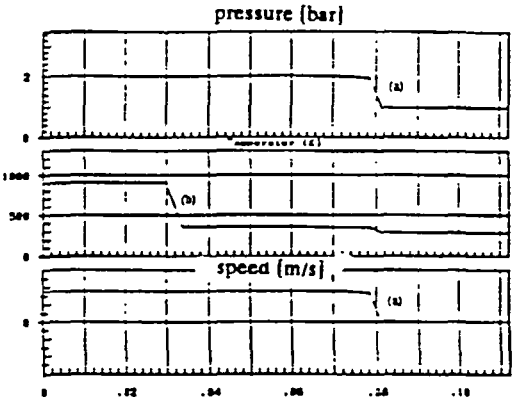

Figure 12

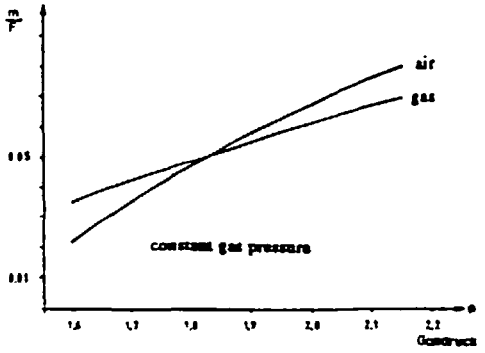

Figure 13

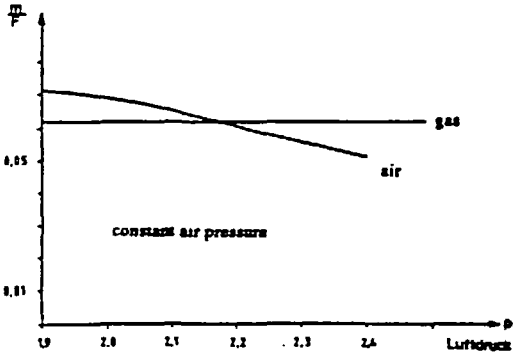

Figure 14

the boundaries of the Comprex. *Figure 13* shows the material flow (gas and air) as a function of the gas pressure in the gas high pressure side. Both curves are computed through numerical simulation of the Comprex for a given constant air pressure. The point of intersection of the two curves represent a balanced operation point for the Comprex motor cycle (0.05 m/F; 1.827 bar). Similar curves were computed for a constant gas pressure (*Figure 14*). A balancing point (0.062 m/F; 2.176 bar) is noted. The stationary and materially balanced operating point of the Comprex-motor circuit needs thus to be computed iteratively by computing the above curves out of Comprex animation. Every point in these figures requires the computation of a complete Comprex cycle. The simple regula falsi algorithm was used to compute the resulting stationary and materially balanced operating point of the Comprex-motor circuit[18].

ACKNOWLEDGEMENT

The authors would like to acknowledge the technical, financial and personal support from ABB, Baden, Switzerland. Dr. I. Elnashar, gas turbine group, ABB, is acknowledged for his scientific support and valuable discussions. Especial acknowledgement is devoted to Mr. A. Mayer (now TTM, Switzerland) for his technical advice and project management.

REFERENCES

1 Jenny, E. *Pressure Charging – Still a Fascinating Task*, C42/82/Mech E (1982)
2 Von Ferson, O. Mit Aufladen Sprit sparen, Mot. Autozeitschrift pp. 100–107 (1982)
3 ABB. Zellenrad für Druckwellenlader, Sonderdruck aus Konstruieren und Gießen, **6**, Nr. 2, pp. 4–6 (1981)
4 Seippel, C. Druckaustauscher, Schweizer Patent Nr. 225 426 (1940)
5 Berchtold, M. and Gardiner, F. J. The Comprex, a New Concept of Diesel Supercharging, Gas Turbine Power Conf. and Exhibition, Washington (1958)
6 Köhnen, L. Comprex Konkurrenz für den Turbolader, Lastauto & Omnibus 46 (1969)
7 Jenny, E. and Bulaty, D. Die Druckwellenmaschine Comprex als Oberstufe einer Gasturbine, MTZ 32, pp. 10–12 (1971)
8 Zehnder, G. Berechnung von Druckwellen in der Aufladertechnik, Brown Boverie Mitt. 4/5 (1971)
9 Daneshyar, H. One-Dimensional Compressible Flow, Oxford, New York, Frankfurt (1976)
10 Kirchhoffer, H. Aufladung von Fahrzeug-Diesel-motoren mit Comprex, Technica 2 (1976)
11 Croes, N. The principle of the pressure wave machine as used for charging Diesel engines, Shock Tube and Shock Wave Research, London, Seattle (1977)
12 Summerauer, H., Spinnler, F., Mayer, C. and Hafner, L. A comparative study of the acceleration performance of a truck diesel engine with the exhaust-gas turbocharger and with pressure-wave supercharger comprex, 1, Mech. Eng. Conf. on Turbocharging and Turbochargers, London (1978)
13 Pfriem, H. Zur Theorie ebener Druckwellen mit steiler Front, Akustische Zeitschrift Sulzer (1941)
14 Schatzmann, J. Beitrag zur Berechnung isentroper eindimensionaler instationärer Gasströmung mit Hilfe von Digitalcomputern, Diss. ETH (1968)
15 Hörler, H. Abschätzung der Verluste in instationär-gasdynamischen Kanaltrommel-Druckaustauschern, Diss. ETH, Zürich (1969)
16 De Haller, P. Über eine graphische Methode in der Gasdynamik, Technische Rundschau Sulzer Nr. 1 (1945)
17 Jenny, E. Berechnung und Modellversuche über Druckwellen großer Amplituden in Auspuffleitungen, Diss. ETH Basel (1949)
18 Oberhem, H. Ein CAD-System für Druckwellenmaschinen, Diss. BUGH Wuppertal (1989)
19 Croes, N. Die Wirkungsweisen der Taschen des Druckwellenladers Comprex, MTZ, 40. Hahrgang Nr. 2 (1979)
20 Nour Eldin, H. A., Oberhem, H. A variable grid for accurate animation of the nonstationary compressible flow in the pressure wave machine, *7th Int. Conf. Num. Meth. in Laminar and Turbulent Flow*, pp. 000–000, Stanford, California, USA (1991)
21 Sauer, R. Einführung in die theoretische Gas-dynamik, Berlin, Göttingen, Heidelberg (1960)
22 Nour Eldin, H. A., Oberhem, H. and Schuster, U. The Variable Grid-Method for Accurate Simulation of Fast Gas Dynamics and Shock-Tube Like Problems, Proc. IMACS/IFFAC *Int. Symp. on Modelling and Simulation of Distributed Parameter Systems*, pp. 241–248, Hiroshima, Japan (1987)